PROCEEDINGS OF SPIE

SPIEDigitalLibrary.org/conference-proceedings-of-spie

Reliability of handheld laser speckle contrast perfusion imaging demonstrated in psoriasis lesions

Chizari, Ata, Schaap, Mirjam, Knop, Tom, Seyger, Marieke M., Steenbergen, Wiendelt

Ata Chizari, Mirjam J. Schaap, Tom Knop, Marieke M. B. Seyger, Wiendelt Steenbergen, "Reliability of handheld laser speckle contrast perfusion imaging demonstrated in psoriasis lesions," Proc. SPIE 11934, Photonics in Dermatology and Plastic Surgery 2022, 119340A (3 March 2022); doi: 10.1117/12.2608663

SPIE.

Event: SPIE BiOS, 2022, San Francisco, California, United States

Downloaded From: https://www.spiedigitallibrary.org/conference-proceedings-of-spie on 25 May 2022 Terms of Use: https://www.spiedigitallibrary.org/terms-of-use

Reliability of handheld laser speckle contrast perfusion imaging demonstrated in psoriasis lesions

Ata Chizari*[a,c], Mirjam J. Schaap[b,c], Tom Knop[a], Marieke M.B. Seyger[b], Wiendelt Steenbergen[a], [a]Biomedical Photonic Imaging, Technical Medical Centre, Faculty of Science and Technology, University of Twente, PO Box 217, 7500 AE Enschede, The Netherlands; [b]Department of Dermatology, Radboud University Medical Center, P.O. Box 9101, 6500 HB Nijmegen, The Netherlands; [c]These authors contributed equally to this work.

ABSTRACT

We assessed the reliability of handheld laser speckle contrast perfusion imaging by evaluating mounted/handheld measurement pairs operated on psoriasis lesions in three steps. First, we made a denoised perfusion map per measurement based on spatial alignment of raw speckle frames and temporal averaging of perfusion frames. Second, we used the measured on-surface speed information to compensate the movement-induced perfusion by extrapolation of the local perfusion values to the value corresponds to zero on-surface speed. Third, we compared mounted/handheld measurement pairs based on perfusion inhomogeneity and increased perilesional perfusion criteria independent of the movement artefact compensation mentioned in the second step. We conclude that after proper post-processing, handheld LSCI measurements can be as reliable as mounted measurements in terms of geometrical distorting, but with challenges to be overcome for correcting perfusion values.

Keywords: laser speckle contrast imaging, psoriasis, handheld, movement artefacts, on-surface speeds, mean separation segmentation, enhanced correlation coefficient maximization, image alignment

1. INTRODUCTION

Laser speckle contrast imaging (LSCI) is a non-invasive method for rapid assessment of relative perfusion [1]. First introduced in 1981, it showed promising capability to visualize blood flow in in-vivo subjects [2]. In this imaging modality, an interference pattern called speckle is imaged with a camera with a certain exposure time (T). Movement of scattering particles such as red blood cells causes the intensity of speckle pattern to fluctuate. The speckle contrast C is calculated as a measure of dynamic level of the speckles resulted by blood flow through the capillaries [3]. The higher the blood flow, the more blurred the imaged speckle pattern and the lower the calculated speckle contrast [4]. Although blood flow is measured in arbitrary units, it has been shown to be linear with that of laser Doppler flowmetry which is known as the utmost quantitative optical approach [5]. There are several methods to calculate speckle contrast such as temporal, spatial or spatiotemporal [6] as well as multi-exposure LSCI [7] that depends on the medical application.

LSCI offers a wide range of medical applications including burns, neurology and ophthalmology [8]. It is an effective tool to evaluate peripheral perfusion in patients with systemic sclerosis [9]. The reproducibility of LSCI perfusion has been recently shown satisfactory when assessing wound healing in mice [10]. A major contribution of LSCI in clinical studies lies in its use during surgery (i.e. intraoperatively). It has recently been shown a promising tool to measure flap perfusion and predict the possibility of postoperative ischemic complications in deep inferior epigastric artery perforator (DIEP) [11].

Apart from the mounted modality, LSCI systems can be operated in handheld mode that brings a number of advantages such as ease of use. In 2014, the first handheld LSCI system based on mobile-phones was introduced [12]. Then, a handheld LSCI system with a focus on point-of-care application was built in 2016 in which a pair of laser and camera were connected to a tablet to perform the processing and show the results [13]. In 2018, a handheld retinal imager was built and was used to image dilated human subjects [14]. At the same year, a camera-phone laser speckle imager was used to study retinal perfusion dysfunction [15]. Recently, Kong et al. showed that a mobile phone camera can make blood flow maps that are

*a.chizari@utwente.nl; phone 31 534 891 225; atachizari.com

Photonics in Dermatology and Plastic Surgery 2022, edited by Bernard Choi, Haishan Zeng,
Proc. of SPIE Vol. 11934, 119340A · © 2022 SPIE · 1605-7422 · doi: 10.1117/12.2608663

Downloaded From: https://www.spiedigitallibrary.org/conference-proceedings-of-spie on 25 May 2022
Terms of Use: https://www.spiedigitallibrary.org/terms-of-use

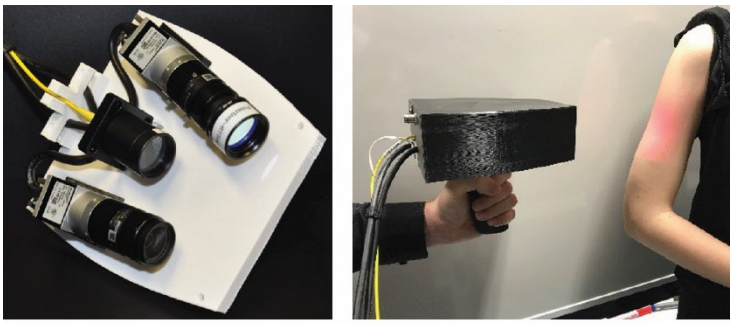

Fig. 1 (a) The probe of the handheld perfusion imager (HAPI) reprinted from [17]. (b) A representative handheld measurement with the HAPI on a healthy test subject.

comparable with that made with an industrial camera [16].

Our recently developed handheld perfusion imager (HAPI), yet mounted on a tripod, showed a promising potential to predict expansion of psoriasis lesions [18]. In a recent study operated on psoriasis lesions, we accomplished fairly similar pairs of mounted/handheld perfusion maps on a visual basis although a significant difference was observed between averaged lesion perfusions of the mounted/handheld pairs [19].

2. RELATED WORKS

A crucial methodological concern with LSCI measurements is movement artefacts due to the underlying sensitivity of speckles to any source of motions. Such motions can be caused by test subjects and/or handheld operation of the system [20]. Mahé et al. were the first to address this challenge by mounting an adjacent opaque surface within the field-of-view (FOV) of speckle images in an attempt to correct the LSCI blood flow maps influence by movement artefacts during involuntarily movements [21] and during a systematic exercise [22]. Richards et al. proposed a combined electrocardiograph (ECG) filtering and image registration method to suppress the influence of both pulsatile flow and respiration on the LSCI blood flow maps obtained intraoperatively after cortical stimulation [23].

Application of an opaque surface within the FOV was further explored by Omarjee et al. who developed an in-house bilayer adhesive that suppressed movement artefacts during handheld LSCI in a more effective manner [24]. Similarly, Lertsakdadet et al. used a fiducial marker imaged at the corner of speckle images obtained by handheld measurements to detect and remove the movement-induced frames as well as tracking of the targeted region-of-interest (ROI) [25]. In another study, they mounted the pair of laser-camera on a motorized stabilizer in order to suppress the amount of applied movements [26]. Recently, Guilbert et al. [27] have regressed out the movement-related signal by identifying a static region in a speckle image. Liu et al. proposed non-rigid registration of temporally averaged perfusion maps during which the imaging object moves. They realized this by simultaneous white-light and laser speckle imaging where the movements were detected employing an optical flow algorithm [28].

In a study of 2020, we explored movement artefacts by measuring the magnitude of movements applied by healthy operators. Then, using motorized measurements on static tissue-mimicking phantoms, we found that on-surface speeds play a more dominant role in speckle contrast drop compared to tilt of wavefronts. We also concluded that optical properties of the medium matters when studying movement artefacts such that a measurement on an opaque surface may not be sufficient to correct for movement artefacts [17]. Then, we studied the influence of wavefront types on movement artefacts in handheld LSCI. We showed that scrambled waves that are used for illumination in commercially available devices cause the highest level of movement artefacts compared to planar and spherical waves [29]. We have also initiated a model based on optical Doppler effect to predict movement artefacts that are caused by translation in a handheld LSCI [30].

In this study, we present two phases of our research on movement artefacts. In the first phase, we propose a method for compensation of movement artefacts during LSCI of psoriasis lesions. The method is based on measurment of on-surface speeds during a handheld operation by tracking of the movements directly on speckle patterns. Then, we connect movement-induced perfusion of each location on a perfusion map to the detected on-surface speeds in order to estimated perfusion at zero-speed. In the second phase, we assess 18 pairs of mounted/handheld perfusion maps on psoriasis lesions

Downloaded From: https://www.spiedigitallibrary.org/conference-proceedings-of-spie on 25 May 2022
Terms of Use: https://www.spiedigitallibrary.org/terms-of-use

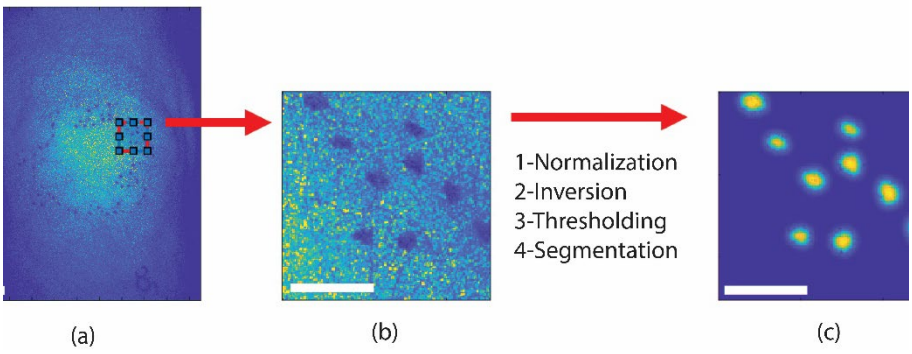

Fig. 2 Procedure of distinguishing marked points within raw speckle frames. (a) manual selection of a region including some marked points in the first speckle frame. (b) The chosen area to follow the indicated 4 steps. The segmentation techniques is called mean-separation [31]. (c) Output of the marker detection procedure. Step (b) is repeated for all the captured frames. Scalebars: 5 mm.

for a clinical point-of-view, namely perfusion inhomogeneity and increased perilesional perfusion already introduced in [18].

3. MATERIALS AND METHODS

The handheld perfusion imager (HAPI) introduced in [19] was used for measurements in both mounted and handheld modalities. The handheld probe without the cap is shown in Fig. 1(a). A representative scenario of a handheld measurement on a healthy subject is shown in Fig. 1(b). The laser source (CNI MSL-FN-671) emits the light with a wavelength of $\lambda = 671$ nm. A single mode optical fiber (Torlabs P1-630A-FC-5) was used to deliver laser light to the handheld probe. The output light from the fiber tip was projected on the tissue using a plano-concave lens (Qioptiq, N-BK 7) where the $1/e^2$ beam width of was about 8 cm at the working distance of about 40 cm. At the detection side, a monochromatic camera (Basler acA2040 55um USB3) operated with a frame rate of $f = 50$Hz, a gain of 10dB and an exposure time of $T = 10$ ms. The camera objective (FUJINON HF16XA5M) had an f-number of F/8. The magnification was calculated as 11.9 px/mm that obtained a field-of-view (FOV) of 12.9 cm × 17.2 cm. A bandpass filter (Edmund Optics) of wavelength 675 ± 12.5 nm followed by a linear polarizer (Thorlabs LPNIRE 100-B) were mounted on the camera objective in order to reduce background noise and specular reflection, respectively.

A physician placed black marker dots (Edding 400, 1 mm, permanent marker) on the clinical psoriatic lesion border in order to provide a reference for the clinically visible lesion borders observed on the perfusion images. Such black marker dots where clearly visible on the raw speckle frames and were used for movement tracking and on-surface speed detection. Subjects were asked to stay still and breath normally while being located in a rest position depending on the skin area to be imaged: sitting or supine. Te operator was conveniently positioned, the arm bent at around 90 ˚ and kept the handheld probe normally (i.e. without any over-concentration). During mounted measurements, the HAPI probe was placed on a tripod.

Each measurement took 7 s during which 350 speckle frames were recorded. The data analysis started by selecting a region of approximately 200 × 200 px on the first raw speckle frame in which a few markers were present. Then, the four steps of normalization, inversion, thresholding and segmentation were applied on the selected region for the consecutive stack of 350 frames. The MATLAB R2019b (Mathworks) software package 'localized active contour' [32] [33] was used that makes image segmentation in the mode of mean separation (MS) [31] [34]. In Fig. 2 this procedure is demonstrated.

The first segmented frame for each stack was made the reference frame for the tracking part. Two-dimensional displacements of the subsequent frames with respect to that reference were calculated by IAT MATLAB R2019b (Mathworks) toolbox [35]. This toolbox performs based on enhanced correlation coefficients maximization (ECC) [36]. The output of the ECC is a 'warp' matrix including horizontal and vertical displacement vectors. This matrix was used for the following two ends; (1) Calculation of on-surface speeds (v_x, v_y) by time derivation of position vectors (x, y) in horizontal and vertical directions and (2) alignment of the raw speckle full frames by translation of each frame according to the associated warp matrix elements in the negative direction. For a demonstration of movement tracking see Fig. 3.

Downloaded From: https://www.spiedigitallibrary.org/conference-proceedings-of-spie on 25 May 2022
Terms of Use: https://www.spiedigitallibrary.org/terms-of-use

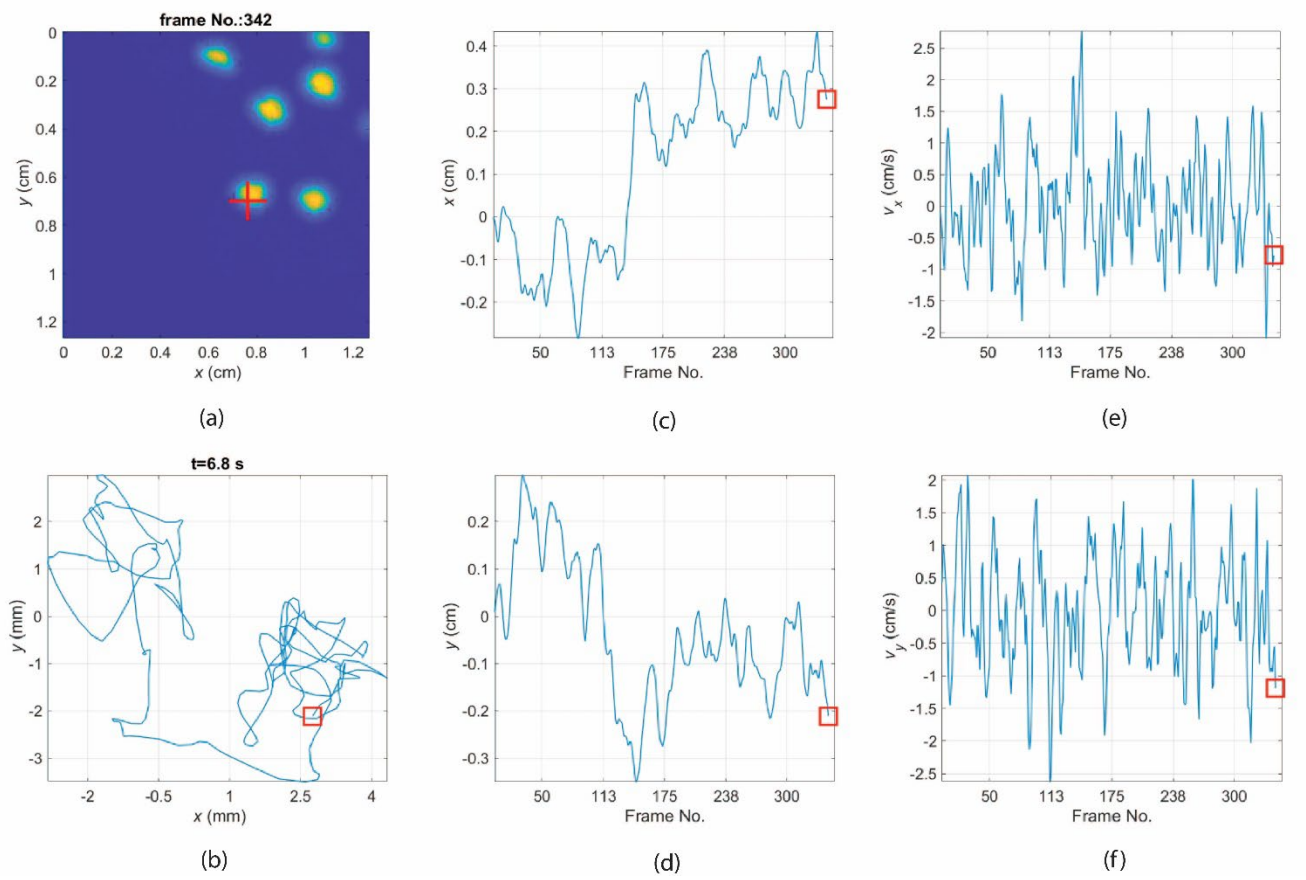

Fig. 3 Motion tracking and calculation of on-surface speeds. (a) Input frames including the marked points. Red cross hair is used to provide a visual comparison of the real movements and output of the tracking algorithm over time (for such visualization see Supplementary Video S2 of [19]). (b) Detected displacements on the $x-y$ plane. (c-d) Detected displacements versus frame number (time) along the $x-$ and $y-$ axis, respectively. (e-f) Calculated on-surface displacements along the $x-$ and $y-$ axis, respectively, by time derivation of the displacements.

The speckle contrast is expressed as $C = \sigma_I/\bar{I}$ where σ_I and $\bar{I}$ are the standard deviation and mean of intensity fluctuations observed by a camera, respectively [37]. In order to convert the raw speckle frames to the so-called contrast maps, a rectangular window spatially sweeps over every raw speckle frame to compute the local speckle contrast values. The algorithm should be implemented with an efficient processing time. Thus, we have used the sliding convolution technique with a rectangular window size of 9×9 px (0.8 mm $\times$ 0.8 mm). This process was repeated for the entire stack of raw speckle frames. After calculation of contrast maps, a look up table was made according to *Step 5* of [19] to assign a perfusion value to each calculated speckle contrast value. This way the so called perfusion maps were made for the entire stack of contrast maps. Finally, the stack of perfusion maps were temporally averaged to make a representative perfusion map per measurement. After this step, the study was followed up in two independent phases that follow in the next two subsections.

3.1 Model of the movement artefact compensation for phase I of the study

In a previous study, we performed motorized experiments during which the HAPI probe was mounted on a translational stage. The speckle contrast was measured on a Delrin plate, forearm of a healthy subject with normal perfusion level and 15 min after application of 0.2 ml vasodilating cream (60 g Midalgan cream Extra Warm, Qualiphar, Meppel, The Netherlands) which formed the case of high perfusion level (see Fig. 4) [19]. When calculating the perfusion values, it turned out that even though the perfusion response to translational speed is linear, its slope tend to increase when the base

Downloaded From: https://www.spiedigitallibrary.org/conference-proceedings-of-spie on 25 May 2022
Terms of Use: https://www.spiedigitallibrary.org/terms-of-use

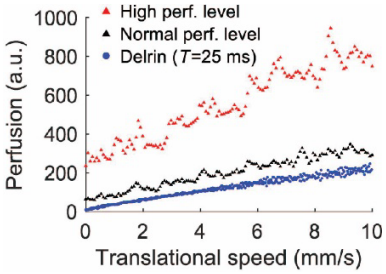

Fig. 4 Perfusion versus translational speed where the handheld LSCI probe is mounted on a translational stage. Data are reprinted from [19]. Perf.: perfusion. The measurements marked with normal and high perf. Levels are performed on the forearm of a healthy subject. High perf. level refers to the measurement 15 minutes after application of Midalgan on the forearm.

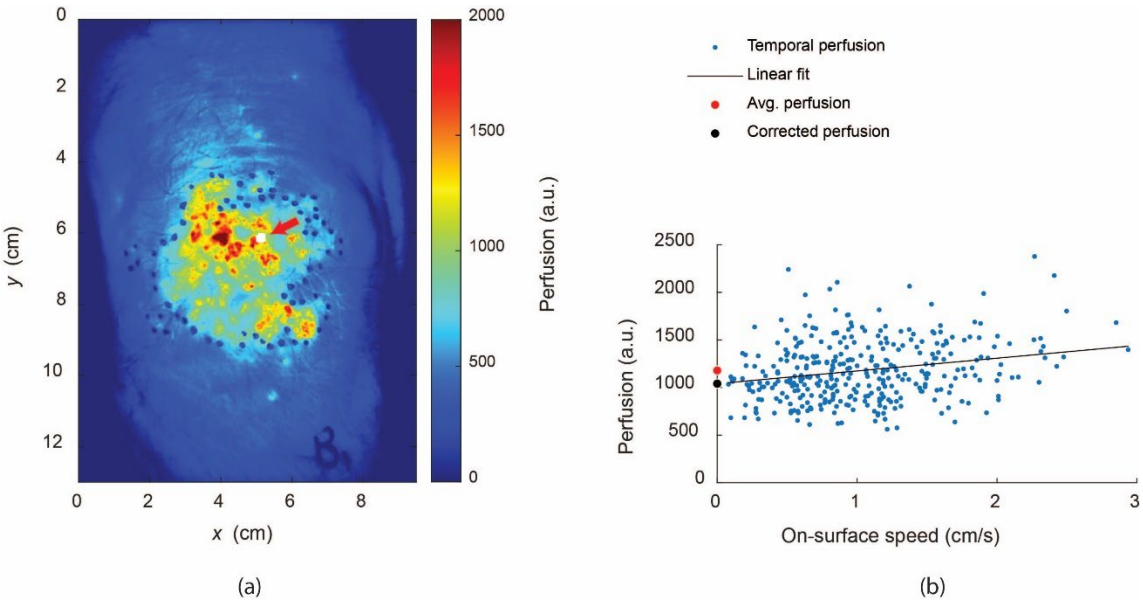

Fig. 5 Representation of movement artefact detection based on the measured on-surface speeds. (a) A spatially aligned and temporally averaged perfusion map of a handheld measurement. (b) Perfusion versus on-surface speed associated with the white area indicated by the red arrow in (a). The red circle is the mean perfusion (mean of the blue points). The black line is a linear interpolation of the blue points. The black point is the y-intercept of the fit line that suggests the movement compensated perfusion. For each location of the white area in (a) a new graph such as (b) is made.

perfusion is higher (base perfusion refers to the perfusion without movement artefact). This means that use of an opaque surface in the FOV and compensating perfusion on that basis would be inaccurate. Therefore, there is a need to develop a robust method of movement artefact compensation.

The time-integrated speckle contrast can be written as follows [30];

$$C^2 = \frac{\tau_c}{2T}\left[2 - \frac{\tau_c}{T}\left(1 - e^{-\frac{2T}{\tau_c}}\right)\right], \tag{1}$$

where τ_c and T are correlation and exposure times, respectively. The correlation time is inversely proportional to applied speed as follows;

$$\tau_c = \frac{1}{v_{\mathrm{RBC}} + v_{\mathrm{ext.}}}, \tag{2}$$

where v_{RBC} and $v_{\mathrm{ext.}}$ are absolute speeds applied by moving red blood cells (RBC) and external sources of speeds that are called movement artefacts. Having knowledge about $v_{\mathrm{ext.}}$ leads to an accurate estimation of v_{RBC} by measurement of time-

Downloaded From: https://www.spiedigitallibrary.org/conference-proceedings-of-spie on 25 May 2022
Terms of Use: https://www.spiedigitallibrary.org/terms-of-use

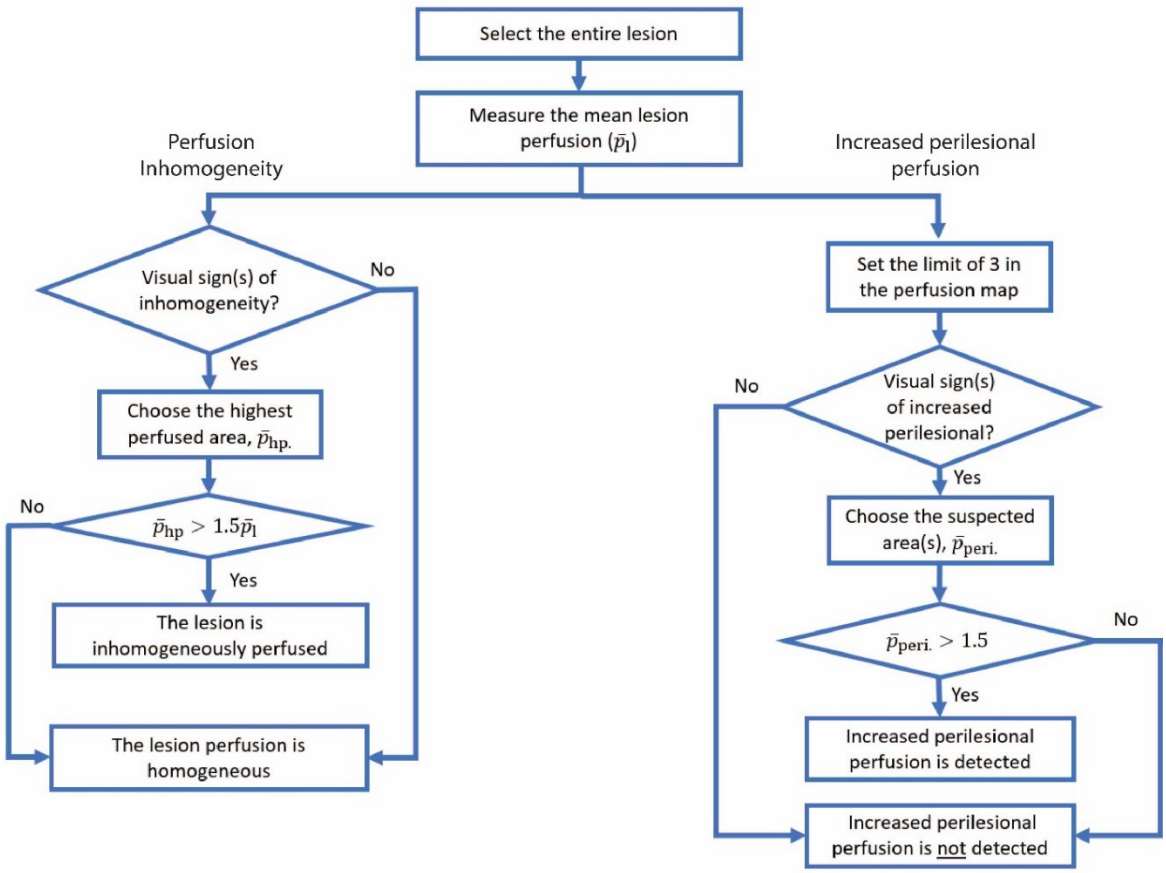

Fig. 6 Flow diagram of the psoriasis lesions analysis. The main branch calculates the mean perfusion of the entire legion. The left branch is dedicated to perfusion inhomogeneity analysis. The output is whether is lesion is inhomogeneously perfused. The right branch is dedicated to increased perilesional perfusion analysis. The output is whether an increased perilesional perfusion is detected (i.e. the lesion is predicted to be expanded).

integrated speckle contrast C. For the phase I of this study, we revisit perfusion maps by creating a lookup table based on (2) and $\tau_c = 1/v_{\mathrm{RBC}}$ since it is the correct equation for the time-integrated speckle contrast compared to what used in *Step 5* of [19].

We propose to relate temporal perfusion at each location of the perfusion map to the detected velocity and assume and calculate the y-intercept of the first-order polynomial fit as zero-speed perfusion. This is equivalent to subtraction of $v_{\mathrm{ext.}}$ from (2) leaving only v_{RBC} as a prediction of tissue perfusion. In Fig. 5, a representative temporally averaged perfusion map and the corresponding curve for estimation of zero-speed perfusion for the determined location is shown.

3.2 Model of the clinical assessment of mounted/handheld pairs for phase II of the study

In this phase of the study, 18 pairs of mounted/handheld perfusion maps where compared from a clinical point-of-view with two criteria, namely perfusion inhomogeneity and increased perilesional perfusion. Prior to introduce each, we mention an extra step after temporal averaging of perfusion maps. This step is called background correction during which three areas on the healthy skin around a lesion is chosen. After calculation of the weighted average of the background perfusion $\bar{p}_b$, the entire perfusion map is divided by $\bar{p}_b$. This way, the region outside of a lesion has an approximately unity perfusion.

In Fig 6, the flow diagram of the clinical assessment is depicted. This assessment is carried out for 18 pairs of mounted/handheld background corrected perfusion maps. The assessment starts by determining perfusion of a lesion. This procedure is done by manually selecting the entire lesion followed by the calculating of weighted lesion average $\bar{p}_l$. Then, the two independent analysis take place. The first analysis the called the perfusion inhomogeneity. The physician inspects a perfusion map and looks for regions with higher perfusion compared to the rest of the lesion. If no region is found, then

Downloaded From: https://www.spiedigitallibrary.org/conference-proceedings-of-spie on 25 May 2022
Terms of Use: https://www.spiedigitallibrary.org/terms-of-use

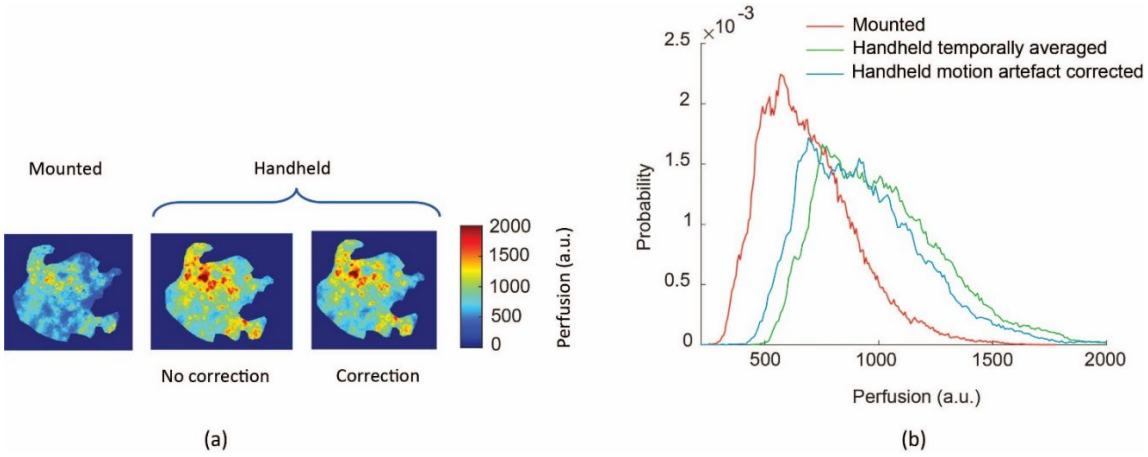

Fig. 7 Results of movement artefact compensation based on measured on-surface speed. (a) A visual comparison between (left) a mounted measurement, (middle) the corresponding handheld measurement affected by movement artefact and (right) the movement artefact corrected version. (b) Probability density functions of the perfusion maps shown in (a).

the lesion perfusion is homogenous. In case of suspecting an area, the perfusion of that area is measured as $\bar{p}_{\mathrm{hp}}$. If $\bar{p}_{\mathrm{hp}}$ is greater than 1.5 times the lesion perfusion $\bar{p}_{\mathrm{l}}$, then the lesion is inhomogeneously perfused.

The second branch of the assessment is called the increase perilesional perfusion. First, a limit of 3 is set to the colorbar of a background corrected perfusion map. This limit helps to highlight relatively low perfusion values outside of a lesion boundary although all the values higher that 3 are saturated. Then, the investigator inspects the signs of increased perilesional perfusion outside of the selected lesion boundary. If no region is found, then increased perilesional perfusion is obviously not detected. In case of suspecting an area, the average perfusion of that area $\bar{p}_{\mathrm{peri.}}$ is calculated. The increased perilesional perfusion is detected only if $\bar{p}_{\mathrm{peri.}}$ is 1.5 times greater than the lesion perfusion $\bar{p}_{\mathrm{l}}$.

4. RESULTS AND DISCUSSION

4.1 Phase I: compensation of movement artefacts

The proposed method for compensation of movement artefacts is applied to a pair of mounted/handheld temporally averaged perfusion maps. Although not zero, the movements of the patient during the pair of measurements is considered negligible such that all the movement artefacts is caused by the movements of the operator during the measurements. Since the lesion perfusion is of focus for the study of movement artefacts, the lesion area is manually selected.

In Fig. 8(a), a comparison between the lesion perfusion of the pair of mounted/handheld measurements is shown. It is evident that due to the movement artefacts, mean lesion perfusion of the handheld measurement is higher than that of mounted measurement. Also, the corresponding perfusion map of the handheld measurement after movement artefact correction is shown. Although not entirely turned back to the mounted version, the movement artefact corrected version does have lower perfusion values compared to its version before the correction on a visual basis.

As a more quantitative comparison, histograms of the three aforementioned perfusion maps are shown in Fig. 8(b). The mounted version clearly has lower mean and standard deviation values. The histogram corresponds to the handheld version without correction has higher mean and standard deviation values compared to the mounted version. It can be seen that the one after movement artefact correction slightly approaches the mounted version which is a promising sign that the proposed method has the potential to effectively correct for movement artefacts.

Results of this phase show that the movement artefacts correction method does not completely recover the handheld version (i.e. the movement artefact corrected handheld measurement does not yet fully match the corresponding mounted version). Therefore, there is room for improvements. Firstly, this method at its current version needs to be tested on a number of mounted/handheld pairs in order to provide a statistical analysis and make a robust conclusion. Secondly, the speed detection is performed directly on the speckle patterns and may be prone to inaccuracies. An alternative would be to perform color imaging parallel with perfusion imaging aiming for accurate speed detection. Thirdly, here a linear

Downloaded From: https://www.spiedigitallibrary.org/conference-proceedings-of-spie on 25 May 2022
Terms of Use: https://www.spiedigitallibrary.org/terms-of-use

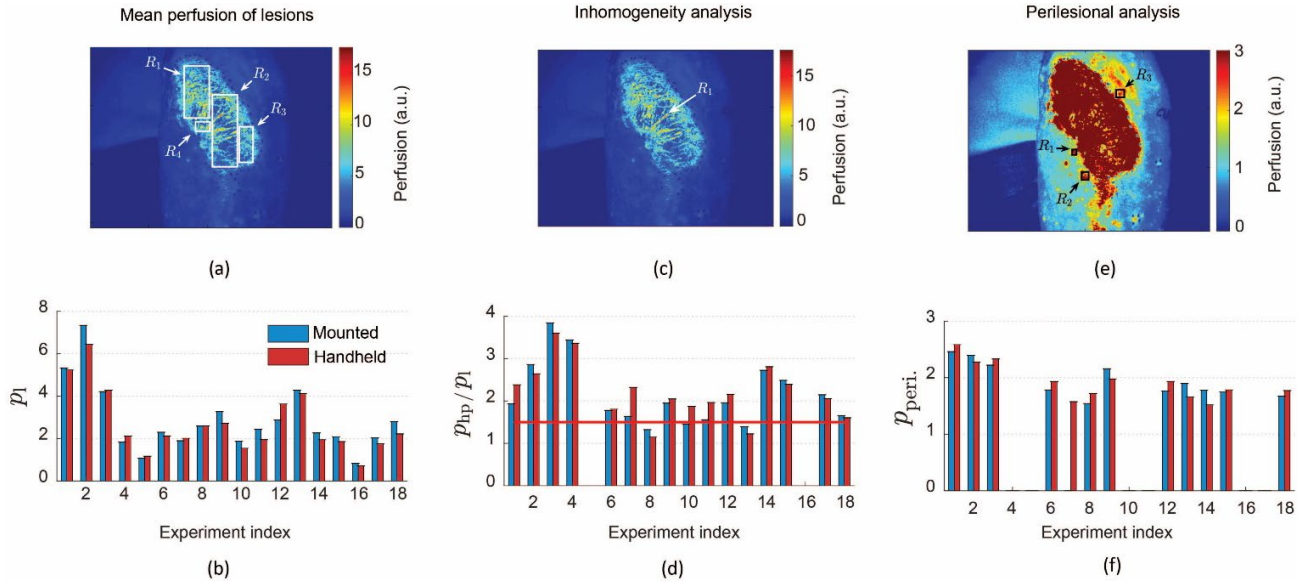

Fig. 8 Results of inhomogeneity and perilesional analysis. (a) Selection of lesion area for a representative psoriasis lesion. (b) A comparison between mean perfusion values of the 18 pairs of mounted/handheld measurements. (c) Exploration of suspected areas with perfusion inhomogeneity. (d) Perfusion of the suspected inhomogeneous areas normalized by the corresponding mean lesion perfusion determined in (b). Horizontal red line: 1.5 threshold. In experiment indices 5 and 16, no suspected areas were found. (e) Selection of suspected 3 perilesional areas (outside of lesion boundaries) of a background corrected perfusion map while the colorbar is limited to 3. (f) Average perfusion of the selected areas with potential perilesional perfusion for the 18 pairs of mounted/handheld measurments.

function is used to fit the local perfusion over time versus the applied speed. However, in practice such relation may not be linear and a second- or a third-order polynomial fit may result in a better movement artefact compensation.

4.2 Phase II: Reliability assessment of mounted/handheld pairs

As explained in Subsection 3.2, an evaluation from a medical point-of-view for eighteen pairs of mounted/handheld perfusion maps was carried out. The results of determination of mean lesion perfusion is illustrated in Fig. 9 (a-b). In the specific case shown in Fig. 9 (a), four regions are chosen to cover the most area of the target lesion with a mean value of 5.3. As shown in Fig. 9 (b), the mean perfusion p_l for the handheld cases are lower than that of mounted due to the movement artefacts. It is worth to note that the mean lesion perfusion values of the temporally averaged handheld perfusion maps are higher than the corresponding mounted ones. After the background correction, these are the handheld ones that are of lower values compared to the mounted ones. The underlying reason is that if the perfusion value in the entire image is increased by a constant value, the relative increasing of the background perfusion, that is low, exceeds the relative increasing of the lesion value, that is high.

The results of perfusion inhomogeneity analysis is depicted in Fig. 9 (c-d). In the representative perfusion map shown in Fig. 9 (c), the suspected region R_1 has a mean perfusion of $p_{hp} = 10.3$ and since it is higher that 1.5 times of the lesion mean perfusion (i.e. $p_l = 5.3$), the lesion is recognized as inhomogeneously perfusion. An overview of the entire measurement pairs with a threshold of 1.5 is shown in Fig. 9 (d). It is seen that except for the experiment index 10, for all measurement pairs both mounted/handheld cases fall either below or above the threshold. This shows a high level of reliability of handheld measurements (even without movement artefact correction) that indicates a consistent result with the associated mounted ones.

The result of the study of increased perilesional perfusion has have been shown in Fig. 9 (e-f). In the representative perfusion maps shown in Fig. 9 (e), three areas are suspected to occur an increased perilesional perfusion. The weighted average for these chosen areas is $p_{peri.} = 2.46$ which is above the threshold of 1.5; therefore, increased perilesional perfusion is detected in this case. The comparison of mounted/handheld pairs for the entire cases is summarized in Fig. 9 (f). It can be clearly seen that either both mounted/handheld cases are above or below the 1.5 threshold except for the experiment index 7 in which no increased perilesional perfusion is suspected for the mounted case. These results confirm

Downloaded From: https://www.spiedigitallibrary.org/conference-proceedings-of-spie on 25 May 2022
Terms of Use: https://www.spiedigitallibrary.org/terms-of-use

the consistency of the handheld measurements (even without correction for movement artefacts) with the corresponding mounted measurements when being analyzed for the increased perilesional perfusion.

5. SUMMARY AND CONCLUSION

In this paper, we assessed the reliability of handheld laser speckle contrast perfusion imaging by evaluating mounted/handheld measurement pairs operated on psoriasis lesions using the developed handheld perfusion imager (HAPI). We applied segmentation and movement tracking on raw speckle frames to measure on-surface displacements of the LSCI system with respect to the test subject, that are caused by involuntarily movements of the handheld operator and/or the patient. Then, we used the on-surface displacement information to compensate the spatial misalignment of the images over time. After that, we created temporally averaged perfusion maps followed by background correction.

First, we showed that the handheld measurements are in agreement with the corresponding mounted measurements on a visual basis. Second, we used the measured on-surface speeds to compensate the movement-induced perfusion by extrapolation of the local perfusion values to the value correspond to zero on-surface speed. This way, the histograms of the perfusion values within lesions in handheld cases after the correction tended to approach the corresponding histograms of mounted cases. This formed the first phase of our study.

Third, we evaluated the mounted/handheld pairs more specifically based on the perfusion inhomogeneity and increased perilesional perfusion criteria, that formed the second phase of our study. In both cases, the handheld measurements of seventeen out of eighteen pairs showed consistent output with the corresponding mounted cases.

We conclude that after proper post-processing, handheld LSCI measurements can be as reliable as mounted measurements for medical assessment of the perfusion in terms of geometrical distorting, but with challenges to be overcome for correcting perfusion values. Enabling reliable handheld LSCI brings convenience for both medical staff and patients.

6. ETHICS DECLARATIONS

All psoriasis participants provided informed consent before enrollment. The ethics committee of the region of Arnhem-Nijmegen and the Radboud university medical center, Nijmegen, the Netherlands (NL69174.091.19) approved the use of the HAPI system and the study protocol. Relevant guidelines and regulations were applied for all experiments.

7. ACKNOWLEDGMENT

This study was supported by the Open Technology program of the Netherlands Organization for Scientific Research (NWO), Domain Applied and Engineering Sciences, under grant number 14538.

8. REFERENCES

[1] D. A. Boas and A. K. Dunn, "Laser speckle contrast imaging in biomedical optics," *Journal of biomedical optics,* vol. 15, p. 011109, 2010.

[2] A. F. Fercher and J. D. Briers, "Flow visualization by means of single-exposure speckle photography," *Optics communications,* vol. 37, p. 326–330, 1981.

[3] J. D. Briers, "Laser Doppler and time-varying speckle: a reconciliation," *JOSA A,* vol. 13, p. 345–350, 1996.

[4] J. D. Briers, "Laser speckle contrast imaging for measuring blood flow.," *Optica Applicata,* vol. 37, 2007.

[5] A. K. Dunn, H. Bolay, M. A. Moskowitz and D. A. Boas, "Dynamic imaging of cerebral blood flow using laser speckle," *Journal of Cerebral Blood Flow & Metabolism,* vol. 21, p. 195–201, 2001.

[6] M. Draijer, E. Hondebrink, T. van Leeuwen and W. Steenbergen, "Review of laser speckle contrast techniques for visualizing tissue perfusion," *Lasers in medical science,* vol. 24, p. 639–651, 2009.

[7] M. Hultman, "Real-time multi-exposure laser speckle contrast imaging of skin microcirculatory perfusion," 2021.

[8] W. Heeman, W. Steenbergen, G. M. van Dam and E. C. Boerma, "Clinical applications of laser speckle contrast imaging: a review," *Journal of biomedical optics,* vol. 24, p. 080901, 2019.

Downloaded From: https://www.spiedigitallibrary.org/conference-proceedings-of-spie on 25 May 2022
Terms of Use: https://www.spiedigitallibrary.org/terms-of-use

[9] M. Di Battista, R. Morganti, E. Tani, M. Da Rio, A. Della Rossa and M. Mosca, "Definition and application of proximal-distal gradient finger perfusion in systemic sclerosis by laser speckle contrast analysis," *Microvascular Research,* p. 104307, 2021.

[10] A. Couturier, R. Bouvet, J.-L. Cracowski and M. Roustit, "Reproducibility of high-resolution laser speckle contrast imaging approaches to assess cutaneous microcirculation for wound healing monitoring in mice," *Microvascular Research,* p. 104319, 2022.

[11] J. Zötterman, D. Opsomer, S. Farnebo, P. Blondeel, S. Monstrey and E. Tesselaar, "Intraoperative laser speckle contrast imaging in DIEP breast reconstruction: a prospective case series study," *Plastic and Reconstructive Surgery Global Open,* vol. 8, 2020.

[12] D. Jakovels, I. Saknite, G. Krievina, J. Zaharans and J. Spigulis, "Mobile phone based laser speckle contrast imager for assessment of skin blood flow," in *Eighth International Conference on Advanced Optical Materials and Devices (AOMD-8)*, 2014.

[13] R. Farraro, O. Fathi and B. Choi, "Handheld, point-of-care laser speckle imaging," *Journal of biomedical optics,* vol. 21, p. 094001, 2016.

[14] A. Rege, S. I. Cunningham, Y. Liu, K. Raje, S. Kalarn, M. J. Brooke, L. Schocket, S. Scott, A. Shafi, L. Toledo and others, "Noninvasive assessment of retinal blood flow using a novel handheld laser speckle contrast imager," *Translational Vision Science & Technology,* vol. 7, p. 7–7, 2018.

[15] I. Remer, L. F. Pierre-Destine, D. Tay, L. M. Golightly and A. Bilenca, "In vivo noninvasive visualization of retinal perfusion dysfunction in murine cerebral malaria by camera-phone laser speckle imaging," *Journal of biophotonics,* vol. 12, p. e201800098, 2019.

[16] P. Kong, H. Xu, R. Li, G. Huang and W. Liu, "Laser Speckle Contrast Imaging Based on a Mobile Phone Camera," *IEEE Access,* vol. 9, p. 76730–76737, 2021.

[17] A. Chizari, T. Knop, B. Sirmacek, F. van der Heijden and W. Steenbergen, "Exploration of movement artefacts in handheld laser speckle contrast perfusion imaging," *Biomedical Optics Express,* vol. 11, p. 2352–2365, 2020.

[18] M. J. Schaap, A. Chizari, T. Knop, H. M. M. Groenewoud, P. E. J. van Erp, E. M. G. J. de Jong, W. Steenbergen and M. M. B. Seyger, "Perfusion measured by laser speckle contrast imaging as a predictor for expansion of psoriasis lesions," *Skin Research and Technology,* 2021.

[19] A. Chizari, M. J. Schaap, T. Knop, Y. E. Boink, M. Seyger and W. Steenbergen, "Handheld versus mounted laser speckle contrast perfusion imaging demonstrated in psoriasis lesions," *Scientific reports,* vol. 11, p. 1–13, 2021.

[20] J. Zötterman, R. Mirdell, S. Horsten, S. Farnebo and E. Tesselaar, "Methodological concerns with laser speckle contrast imaging in clinical evaluation of microcirculation," *PLoS ONE,* vol. 12, p. 1–11, 2017.

[21] G. Mahé, P. Rousseau, S. Durand, S. Bricq, G. Leftheriotis and P. Abraham, "Laser speckle contrast imaging accurately measures blood flow over moving skin surfaces," *Microvascular research,* vol. 81, p. 183–188, 2011.

[22] G. Mahé, P. Abraham, A. Le Faucheur, A. Bruneau, A. Humeau-Heurtier and S. Durand, "Cutaneous microvascular functional assessment during exercise: a novel approach using laser speckle contrast imaging," *Pflügers Archiv-European Journal of Physiology,* vol. 465, p. 451–458, 2013.

[23] L. M. Richards, E. L. Towle, D. J. Fox and A. K. Dunn, "Intraoperative laser speckle contrast imaging with retrospective motion correction for quantitative assessment of cerebral blood flow," *Neurophotonics,* vol. 1, p. 015006, August 2014.

[24] L. Omarjee, I. Signolet, A. Humeau-Heutier, L. Martin, D. Henrion and P. Abraham, "Optimisation of movement detection and artifact removal during laser speckle contrast imaging," *Microvascular research,* vol. 97, p. 75–80, 2015.

[25] B. Lertsakdadet, B. Y. Yang, C. E. Dunn, A. Ponticorvo, C. Crouzet, N. Bernal, A. J. Durkin and B. Choi, "Correcting for motion artifact in handheld laser speckle images," *Journal of Biomedical Optics,* vol. 23, p. 1, 2018.

[26] B. Lertsakdadet, C. Dunn, A. Bahani, C. Crouzet and B. Choi, "Handheld motion stabilized laser speckle imaging," *Biomedical Optics Express,* vol. 10, p. 5149, 2019.

[27] J. Guilbert and M. Desjardins, "Movement correction method for laser speckle contrast imaging of cerebral blood flow in cranial windows in rodents," *Journal of Biophotonics,* p. e202100218, 2021.

Downloaded From: https://www.spiedigitallibrary.org/conference-proceedings-of-spie on 25 May 2022
Terms of Use: https://www.spiedigitallibrary.org/terms-of-use

[28] X. Liu, J. Wei, L. Meng, W. Cheng, X. Zhu, J. Lu and P. Li, "Motion correction of laser speckle imaging of blood flow by simultaneous imaging of tissue structure and non-rigid registration," *Optics and Lasers in Engineering,* vol. 140, p. 106526, 2021.

[29] A. Chizari, T. Knop, W. Tsong, S. Schwieters and W. Steenbergen, "Influence of wavefront types on movement artefacts in handheld laser speckle contrast perfusion imaging," *OSA Continuum,* vol. 4, p. 1875–1888, 2021.

[30] A. Chizari, "Handheld laser speckle contrast perfusion imaging," University of Twente, Netherlands, 2021.

[31] S. Lankton and A. Tannenbaum, "Localizing Region-Based Active Contours," *IEEE Transactions on Image Processing,* vol. 17, p. 2029–2039, November 2008.

[32] Jincheng Pang, *Localized Active Contour,* 2014.

[33] C. Li, C.-Y. Kao, J. C. Gore and Z. Ding, "Minimization of Region-Scalable Fitting Energy for Image Segmentation," *IEEE Transactions on Image Processing,* vol. 17, p. 1940–1949, October 2008.

[34] A. Yezzi, A. Tsai and A. Willsky, "A statistical approach to snakes for bimodal and trimodal imagery," in *Proceedings of the Seventh IEEE International Conference on Computer Vision*, 1999.

[35] G. Evangelidis, *IAT: A Matlab toolbox for image alignment,* 2013.

[36] G. D. Evangelidis and E. Z. Psarakis, "Parametric Image Alignment Using Enhanced Correlation Coefficient Maximization," *IEEE Transactions on Pattern Analysis and Machine Intelligence,* vol. 30, pp. 1858-1865, 2008.

[37] J. W. Goodman, Speckle phenomena in optics: theory and applications, Roberts and Company Publishers, 2007.

Downloaded From: https://www.spiedigitallibrary.org/conference-proceedings-of-spie on 25 May 2022
Terms of Use: https://www.spiedigitallibrary.org/terms-of-use